TRAJECTORY TRACKING CONTROL OF A TWO-LINK ROBOT MANIPULATOR USING VARIABLE STRUCTURE SYSTEM THEORY

Florin Moldoveanu, Vasile Comnac, Dan Floroian, Cristian Boldisor

Department of Automation, TRANSILVANIA University of Brasov
500036 Brasov, Romania
e-mail: moldof@marconi.unitbv.ro, web page: http://www.unitbv.ro

***Abstract**. The control of robots, mobile robots and manipulator arms has fascinated control engineers for several decades. Robots are complex mechanical systems with highly nonlinear dynamics. Hence high-performance operation requires nonlinear control designs to fully exploit a robot's capabilities. After describing the dynamic model for robot, in this paper, we discuss sliding mode control design alternative for the classic trajectory tracking problem, in which the robot is asked to follow a prescribed trajectory. Finally, we will illustrated the control method on a computer simulated example of a two-link robot manipulator.*

***Keywords**: Robot control, variable structure system, sliding mode control, trajectory tracking control.*

1. INTRODUCTION

A large number of control problems for mechanical systems are based on controlling the position or location of a mass using a force or a torque as the input variable. Instead of the pure regulation problem of driving the output location to a specified value, the position of the mass is often required to follow a prescribed trajectory. Levels of complexity may be added by introducing sets of masses with coupled dynamics, to be controlled by sets of force/torque inputs. The standard "fully actuated" case then features one control force/torque input associated with each primary mass and additional forces/torques arising from static and dynamic coupling between the different masses. A typical example is a robotic arm or robot manipulator with n links connected by n joints with force/torque generating actuators. Usually, an end effector tool is mounted at the tip of the last link for manipulating objects according to the specific robot application. The input forces/torques are the outputs of actuators, often electrical actuators, with their own complex dynamics. These actuator dynamics are usually neglected in the first step of control design for the electromechanical system, assuming they are stable and considerably faster than the inertial dynamics of the masses. Also, other dynamics such as structural flexibilities are often neglected when deriving a basic model for the mechanical system.

For the purpose of general control design considerations in the first part of this paper, consider a continuous-time model of a generic, fully actuated n-dimensional robotic system with inertial dynamics of the form [2,5,7]:

$$\boldsymbol{M}(\boldsymbol{q})\ddot{\boldsymbol{q}} + \boldsymbol{N}(\boldsymbol{q},\dot{\boldsymbol{q}}) = \tau , \qquad (1)$$

where $\boldsymbol{q} \in \boldsymbol{R}^{n\times 1}$ is a vector of generalized configuration variables (translational or rotational), $\boldsymbol{M}(\boldsymbol{q}) \in \boldsymbol{R}^{n\times n}$ denotes an inertial mass matrix, $\boldsymbol{N}(\boldsymbol{q},\dot{\boldsymbol{q}}) \in \boldsymbol{R}^{n\times 1}$ comprises coupling forces/ torques between the masses as well as gravity and friction, and $\tau \in \boldsymbol{R}^{n\times 1}$ is a vector of generalized external (input) forces/torques (excluding gravity). Equation (1) describes the principal relationship between inertial motion of the system masses, internal forces/torques $\boldsymbol{N}(\boldsymbol{q},\dot{\boldsymbol{q}})$ and external input forces/torques τ, hence it is well suited for control design.

Traditionally, robots have been categorized into *robot manipulator* and *mobile robots*. Robot manipulators usually have a fixed base and consist of a number of rigid links, connected by translatory or rotatory joints. A set of $\boldsymbol{q} \in \boldsymbol{R}^{n\times 1}$ configuration variables of the *n* joints prescribes a robot configuration, also called robot posture. The set of all possible configurations within the physical joint limitations defines the robot configuration space. The robot *kinematics* provide a mapping between joint coordinates and world coordinates. The associated locations of a given point of the manipulator, e.g. the tip of its end effector in a world coordinate system, define the robot workspace. Note that multiple configurations may result in similar end effector positions. Consequently, the inverse kinematic mapping between end effector location in world coordinates and the configuration vector $\boldsymbol{q} \in \boldsymbol{R}^{n\times 1}$ is not unique, so we omit the treatment of *inverse kinematics* and concentrate on control design in configuration space.

For control design, we distinguish *holonomic* and *nonholonomic* robots [3]. The motion of a holonomic robot is usually unconstrained. All joints may move arbitrarily within their physical limitations and the constraints of the robot workspace, i.e. only limits of the position variables exist.

2. 2 HOLONOMIC ROBOT MODEL

A well-known example of highly nonlinear, fully actuated mechanical systems with coupled dynamics is a robot manipulator with rigid links. For a large class of holonomic robot systems, the generic dynamics in (1) can be rewritten in configuration space as [2,5,7,8]:

$$\boldsymbol{M}(\boldsymbol{q})\ddot{\boldsymbol{q}} + \boldsymbol{V}_m(\boldsymbol{q},\dot{\boldsymbol{q}})\dot{\boldsymbol{q}} + \boldsymbol{F}(\dot{\boldsymbol{q}}) + \boldsymbol{G}(\boldsymbol{q}) = \tau \,, \qquad (2)$$

where $\boldsymbol{q} \in \boldsymbol{R}^{n\times 1}$ denotes the joint configurations (translational or rotational) of the *n* robot links, $\boldsymbol{M}(\boldsymbol{q})$ stands for the inertial mass matrix, $\boldsymbol{V}_m(\boldsymbol{q},\dot{\boldsymbol{q}}) \in \boldsymbol{R}^{n\times n}$ comprises Coriolis and centripetal forces, vector $\boldsymbol{F}(\dot{\boldsymbol{q}}) \in \boldsymbol{R}^{n\times 1}$ describes viscous friction and vector $\boldsymbol{G}(\boldsymbol{q}) \in \boldsymbol{R}^{n\times 1}$ contains the gravity terms. The formulation (2) follows directly from the Euler-Lagrange equations of motion and encompasses robot manipulators operating freely without motion constraints.

The square mass matrix $\boldsymbol{M}(\boldsymbol{q})$ is symmetric, positive definite, and can be written as:

$$\boldsymbol{M}(\boldsymbol{q}) = \begin{bmatrix} m_{11}(\boldsymbol{q}) & \cdots & m_{1n}(\boldsymbol{q}) \\ \vdots & \ddots & \vdots \\ m_{n1}(\boldsymbol{q}) & \cdots & m_{nn}(\boldsymbol{q}) \end{bmatrix}, \qquad (3)$$

with bounded parameters $m_{ij}^{-} \le m_{ij}(\boldsymbol{q}) \le m_{ij}^{+}$, $1 \le i$, $j \le n$. Hence $\boldsymbol{M}(\boldsymbol{q})$ can be bounded by:

$$M^{-} \le \left\|\boldsymbol{M}(\boldsymbol{q})\right\|_2 \le M^{+}\,, \qquad (4)$$

where any induced matrix norm may be used to define two known scalars $0 < M^{-} \le M^{+}$ as bounds. The known scalars M^{-} and M^{+} also bound the inverse of $\boldsymbol{M}(\boldsymbol{q})$:

$$\frac{1}{M^{+}} \le \left\|\boldsymbol{M}^{-1}(\boldsymbol{q})\right\|_2 \le \frac{1}{M^{-1}}\,. \qquad (5)$$

In (4) and in the sequel, the induced 2-norm will be used as an example of bounding norms, but many other norms may be employed instead. The induced 2-norm of matrix $\boldsymbol{M}(\boldsymbol{q})$ is defined as [7]:

$$\left\|\boldsymbol{M}(\boldsymbol{q})\right\|_2 = \sqrt{\max\{\lambda(\boldsymbol{M}^T\boldsymbol{M})\}}\,, \qquad (6)$$

where $\lambda(\boldsymbol{M}^T\boldsymbol{M})$ denotes the eigenvalues of matrix $\boldsymbol{M}^T\boldsymbol{M}$.

The time derivative of the mass matrix, $\dot{\boldsymbol{M}}(\boldsymbol{q}) = \mathrm{d}\,\boldsymbol{M}(\boldsymbol{q})/\mathrm{d}t = (\partial\boldsymbol{M}(\boldsymbol{q})/\partial\boldsymbol{q})\dot{\boldsymbol{q}}$, and the Coriolis/centripetal matrix, $\boldsymbol{V}_m(\boldsymbol{q},\dot{\boldsymbol{q}})\dot{\boldsymbol{q}}$, are skew symmetric, i.e.:

$$\boldsymbol{y}^T(\dot{\boldsymbol{M}}(\boldsymbol{q}) - 2\boldsymbol{V}_m(\boldsymbol{q},\dot{\boldsymbol{q}}))\boldsymbol{y} = 0\,, \qquad (7)$$

holds for any nonzero vector $\boldsymbol{y} \in \boldsymbol{R}^{n\times 1}$.

The Coriolis/centripetal vector $\boldsymbol{V}_m(\boldsymbol{q},\dot{\boldsymbol{q}})\dot{\boldsymbol{q}}$ is bounded by:

$$\|\boldsymbol{V}_m(\boldsymbol{q},\dot{\boldsymbol{q}})\dot{\boldsymbol{q}}\|_2 \le V^+\|\dot{\boldsymbol{q}}\|_2, \quad (8)$$

where V_m^+ is a positive scalar. Viscous friction may be bounded by positive scalars F^+ and F_0:

$$\|\boldsymbol{F}(\dot{\boldsymbol{q}})\|_2 \le F^+\|\dot{\boldsymbol{q}}\|_2 + F_0. \quad (9)$$

The gravity vector likewise is bounded by a positive scalar G^+:

$$\|\boldsymbol{G}(\boldsymbol{q})\|_2 \le G^+. \quad (10)$$

2.1 Holonomic model of a two-link manipulator

A planar, two-link manipulator with revolute joints will be used as an example throughout the control development in Section 3 (see Fig. 1) [7,8]. The manipulator and the associated variables are depicted in Figure 2. The geometry in Figure 2 reveals the *forward kinematics* of the two-link manipulator. The end effector position (x_2, y_2), i.e. the location of mass M_2 in world coordinate frame (x, y), is given by:

$$\begin{aligned} x_2 &= L_1 \cos q_1 + L_2 \cos(q_1+q_2), \\ y_2 &= L_1 \sin q_1 + L_2 \sin(q_1+q_2), \end{aligned} \quad (11)$$

where q_1, q_2 denote the joint displacements and L_1, L_2 are the link lengths.

Solving (11) for the joint displacements as a function of the end effector position (x_2, y_2) yields the *inverse kinematics* as:

$$\begin{aligned} q_1 &= \operatorname{atan2}(y_2, x_2) - \\ &\quad - \operatorname{atan2}(L_2 \sin q_2, L_1 + L_2 \cos q_2), \end{aligned} \quad (12)$$

$$q_2 = \operatorname{atan} 2(D, C),$$

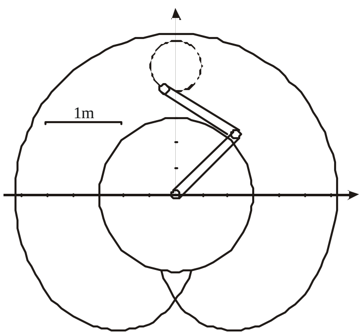

Fig. 1. Circular trajectory in the Cartesian space.

with:

$$C = \frac{x_2^2 + y_2^2 - L_1^2 - L_2^2}{2L_1^2 L_2^2},$$

$$D = \pm\sqrt{1-C^2},$$

which is obviously not unique due to the two sign options of the square root in variable D. The function atan2(·) describes the arctan func-tion normalized to the range ± 180^0.

Applying a standard modelling technique such as the Euler-Lagrange equations yields the dynamic model according to (1) as:

$$\begin{bmatrix} \tau_1 \\ \tau_2 \end{bmatrix} = \begin{bmatrix} m_{11} & m_{12} \\ m_{21} & m_{22} \end{bmatrix} \begin{bmatrix} \ddot{q}_1 \\ \ddot{q}_2 \end{bmatrix} + \begin{bmatrix} n_1 \\ n_2 \end{bmatrix}, \quad (13)$$

$$\boldsymbol{M}(\boldsymbol{q}) = \begin{bmatrix} m_{11} & m_{12} \\ m_{21} & m_{22} \end{bmatrix}, \; \boldsymbol{N}(\boldsymbol{q},\dot{\boldsymbol{q}}) = \begin{bmatrix} n_1 \\ n_2 \end{bmatrix} \quad (14)$$

with:

$$m_{22} = L_2^2 M_2,$$

$$m_{12} = m_{21} = m_{22} + L_1 L_2 M_2 \cos q_2,$$

$$m_{11} = L_1^2(M_1 + M_2) + 2m_{12} - m_{22},$$

$$n_2 = L_1 L_2 M_2 \dot{q}_1^2 \sin q_2,$$

$$n_1 = -L_1 L_2 M_2 (2\dot{q}_1\dot{q}_2 - \dot{q}_2^2) \sin q_2.$$

Table 1: Two-link manipulator parameters.

M_1 = 10kg	M_2 = 1kg
L_1 = 1m	L_2 = 1m

Note the absence of gravity terms in (14) since the manipulator is operated in the plane, perpendicular to gravity. For the control design example in the following section, we will use the parameters in Table 1.

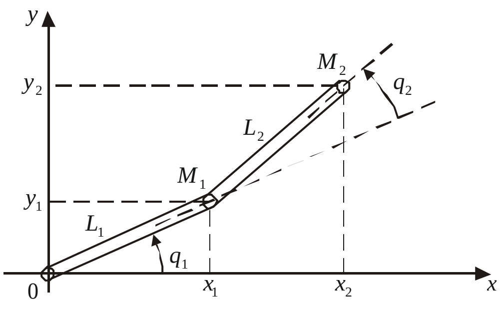

Fig. 2. Two-link manipulator with link lengths L_1 and L_2, and concentrated link masses M_1 and M_2.

The manipulator is shown in joint confi-guration (q_1, q_2), which leads to end effector position (x_2, y_2) in world coordinates. The manipulator is operated in the plane, i.e. gravity acts along the z-axis.

To examine the skew symmetry property in equation (7), take the derivative of mass matrix $\boldsymbol{M}(\boldsymbol{q})$ in (14) to yield:

$$\dot{\boldsymbol{M}}(\boldsymbol{q},\dot{\boldsymbol{q}}) = \begin{bmatrix} 2\dot{m}_{12} & \dot{m}_{12} \\ \dot{m}_{12} & 0 \end{bmatrix}, \tag{15}$$

with:

$\dot{m}_{12}(\boldsymbol{q},\dot{\boldsymbol{q}}) = L_1 L_2 M_2 \dot{q}_2 \sin q_2$.

Then separate matrix $\boldsymbol{N}(\boldsymbol{q},\dot{\boldsymbol{q}})$ into its components according to (2). Due to the assumptions of planar operation and no friction, the gravity and friction terms are equal to zero and we obtain:

$$\boldsymbol{N}(\boldsymbol{q},\dot{\boldsymbol{q}}) = \boldsymbol{V}(\boldsymbol{q},\dot{\boldsymbol{q}}) = \boldsymbol{V}_m(\boldsymbol{q})\dot{\boldsymbol{q}},$$

$$\boldsymbol{V}_m(\boldsymbol{q}) = \begin{bmatrix} V_{m11} & V_{m12} \\ V_{m21} & 0 \end{bmatrix}, \tag{16}$$

where:

$V_{m11} = -L_1 L_2 M_2 \dot{q}_2 \sin q_2$,

$V_{m12} = -L_1 L_2 M_2 (\dot{q}_1 + \dot{q}_2) \sin q_2$,

$V_{m21} = L_1 L_2 M_2 \dot{q}_1 \sin q_2$.

Skew symmetry follows from (15) and (16) as:

$$\begin{aligned} \boldsymbol{y}^T(\dot{\boldsymbol{M}}(\boldsymbol{q}) - 2\boldsymbol{V}_m(\boldsymbol{q},\dot{\boldsymbol{q}}))\boldsymbol{y} &= \\ &= L_1 L_2 M_2 \sin q_2 [y_1 \quad y_2] \cdot \end{aligned} \tag{17}$$

$$(\boldsymbol{A} - 2\boldsymbol{B})\boldsymbol{y} = L_1 L_2 M_2 \sin q_2 \boldsymbol{y}^T(\boldsymbol{C}) \begin{bmatrix} y_1 \\ y_2 \end{bmatrix} = 0,$$

where:

$$\boldsymbol{A} = \begin{bmatrix} -2\dot{q}_2 & -\dot{q}_2 \\ -\dot{q}_2 & 0 \end{bmatrix},$$

$$\boldsymbol{B} = \begin{bmatrix} -\dot{q}_2 & -\dot{q}_1 - \dot{q}_2 \\ \dot{q}_1 & 0 \end{bmatrix},$$

$$\boldsymbol{C} = \begin{bmatrix} 0 & 2\dot{q}_1 + \dot{q}_2 \\ -2\dot{q}_1 - \dot{q}_2 & 0 \end{bmatrix},$$

$$\boldsymbol{y} = \begin{bmatrix} y_1 \\ y_2 \end{bmatrix}.$$

Assuming exact knowledge of the parameters in Table 1, but ignoring all dependencies on joint positions, we can find upper and lower bounds for the elements of the matrices $\boldsymbol{M}(\boldsymbol{q})$ and $\boldsymbol{N}(\boldsymbol{q},\dot{\boldsymbol{q}})$ in (14); they are listed in Table 2. Using the 2-norm according to (6) results in upper and lower bounds for mass matrix $\boldsymbol{M}(\boldsymbol{q})$ as described in (4): $M^- = 0{,}957\ \mathrm{kg\,m}^2$ and $M^+ = 204{,}511\ \mathrm{kg\,m}^2$. Matrix $\boldsymbol{N}(\boldsymbol{q},\dot{\boldsymbol{q}})$ can be upper bounded as $N^+ = (2|\dot{q}_1\dot{q}_2| + \dot{q}_2^2) \times 1\ \mathrm{kg\,m}^2$.

Table 2: Lower and upper bounds of matrix elements.

$m_{11}^- = 12\ \mathrm{kg\,m}^2$	$m_{11}^+ = 14\ \mathrm{kg\,m}^2$
$m_{12}^- = m_{21}^- = 1\ \mathrm{kg\,m}^2$	$m_{12}^+ = m_{21}^+ = 2\ \mathrm{kg\,m}^2$
$m_{22}^- = 1\ \mathrm{kg\,m}^2$	$m_{22}^+ = 1\ \mathrm{kg\,m}^2$
$n_1^+ = (2\lvert\dot{q}_1\dot{q}_2\rvert + \dot{q}_2^2) \times 1\ \mathrm{kg\,m}^2$	
$n_2^+ = \dot{q}_2^2 \times 1\ \mathrm{kg\,m}^2$	

3. TRAJECTORY TRACKING CONTROL

The control task commonly arising in robot control is to track a time-dependent trajectory described by:

$$[\boldsymbol{q}_d(t)\ \dot{\boldsymbol{q}}_d(t)\ \ddot{\boldsymbol{q}}_d(t)], \tag{18}$$

with bounded desired configurations: $\boldsymbol{q}_d(t) = [q_{d_1}(t),\ldots,q_{d_i}(t),\ldots,q_{d_n}(t)]$, velocities: $\dot{\boldsymbol{q}}_d(t) = [\dot{q}_{d_1}(t),\ldots,\dot{q}_{d_i}(t),\ldots,\dot{q}_{d_n}(t)]$ and accelerations: $\ddot{\boldsymbol{q}}_d(t) = [\ddot{q}_{d_1}(t),\ldots,\ddot{q}_{d_i}(t),\ldots,\ddot{q}_{d_n}(t)]$, for each component of an n-dimensional system like (1). Control of a second-order mechanical system with a force/torque input as in (1), requires position and velocity feedback as a basis for stabilization, i.e. PD-type control. This requirement can either be met by measurement and feedback of both position and velocity variables or by a lead compensator for position measurements in the linear sense. In sliding mode control designs, this requirement is reflected in the choice of the sliding manifold with a stable motion, designed as a (linear) combination of position and velocity variables [2,5,6,8,9].

3.1 Circular trajectory for planar two-link manipulator

For the control design examples in this section, we will take the planar two-link manipulator of Section 2.1 and require it to follow a circular trajectory in its workspace. The circle with centre (x_d, y_d) and radius r_d is given in world coordinates (x, y) by:

$$\begin{aligned} x_d(t) &= x_{d_0} + r_d \cos \Psi_d, \\ y_d(t) &= y_{d_0} - r_d \sin \Psi_d, \end{aligned} \tag{19}$$

$$\Psi_d(t) = \frac{2\pi}{t_f}t - \sin\left(\frac{2\pi}{t_f}t\right), \; (0 \le t \le t_f).$$

The operation is assumed to start at time $t = 0$ and to be completed at final time $t = t_f$. The parameters for the examples are listed in Table 3.

Table 3: Parameters of desired circular trajectory.

$x_d = 1\,\text{m}$	$y_d = 1\,\text{m}$
$r_d = 0{,}5\,\text{m}$	$t_f = 5\,\text{s}$

Bounds over the time interval $0 \le t \le t_f$ can be obtained using the inverse kinematics (12) as summarized in Table 4. The desired trajectory is depicted in Figure 3.

3.2 *Vector control*

For some systems, in particular for those with control input vector components are bound $(-\tau_{0_i} \le \tau_i \le +\tau_{0_i},\; i = 1,\ldots,n)$, *vector control* is an elegant alternative.

Table 4: Bounds of desired circular trajectory.

$\lvert\Psi_d\rvert \le \frac{2\pi}{5}$	$\lvert\dot{\Psi}_d\rvert \le \frac{4\pi}{5}$	$\lvert\ddot{\Psi}_d\rvert \le \frac{4\pi^2}{25}$
$\lvert\dot{q}_{d_1}\rvert \le 1\,\text{rad s}^{-1}$	$\lvert\dot{q}_{d_2}\rvert \le 1\,\text{rad s}^{-1}$	

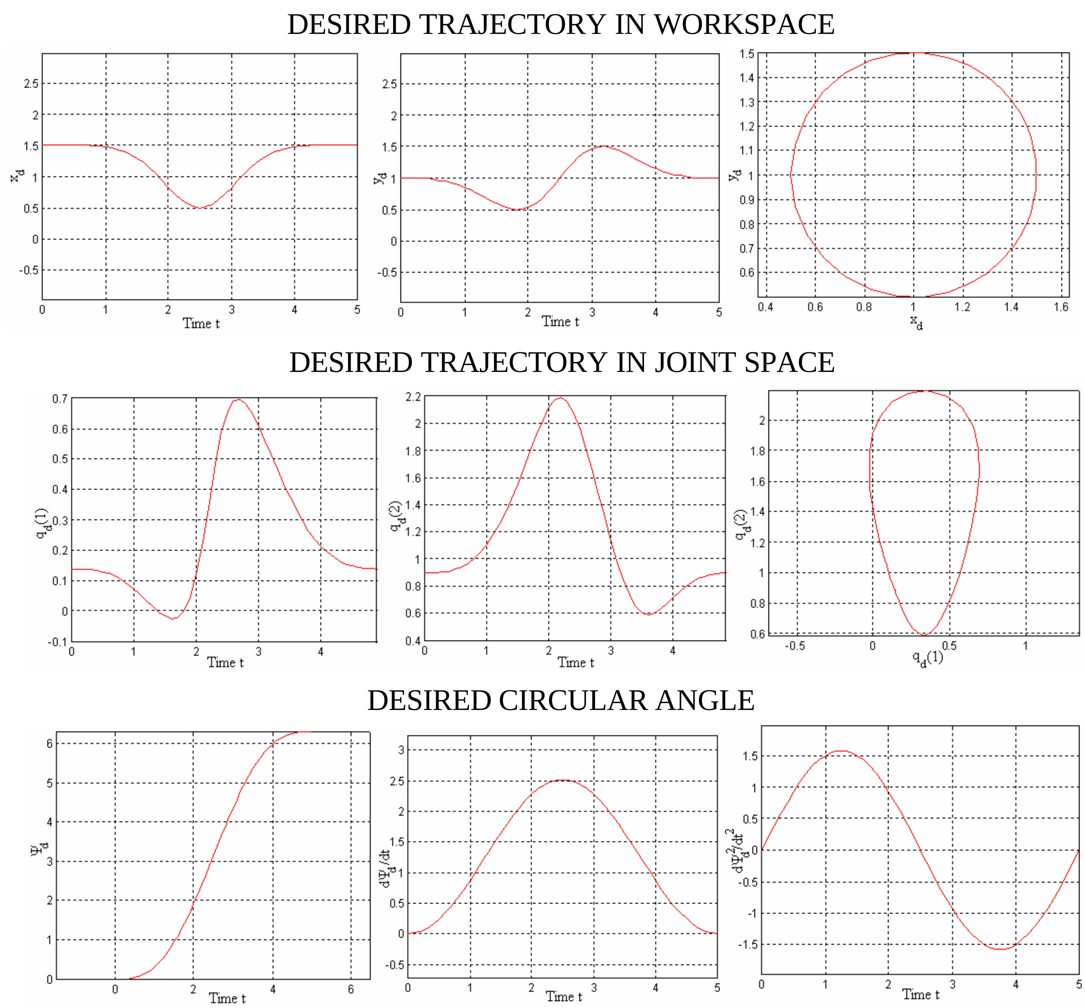

Fig. 3. Desired circular trajectories for control examples. Top row: workspace trajectory in world coordinates (x, y). Middle row: associated joint space trajectory in (q_1, q_2) coordinates. Bottom row: time trajectory of angle Ψ_d.

In contrast to the set of n one-dimensional sliding manifolds $s_i = 0$ for other control design methods, vector control is based on a single n-dimensional vector sliding manifold [6]:

$$\boldsymbol{s} = \boldsymbol{C}\boldsymbol{q}_e + \dot{\boldsymbol{q}}_e\,,\ (\boldsymbol{s} \in \boldsymbol{R}^{n\times 1})\,, \tag{20}$$

where $\boldsymbol{C} \in \boldsymbol{R}^{n\times n}$ is a Hurwitz and preferably diagonal gain matrix, $\boldsymbol{q}_e(t) = \boldsymbol{q}_d(t) - \boldsymbol{q}(t)$ is the tracking error vector, and input vector t is defined as:

$$\mathrm{t} = \tau_0 \frac{\boldsymbol{s}}{\|\boldsymbol{s}\|_2}\,,\ (\mathrm{t} \in \boldsymbol{R}^{n\times 1})\,. \tag{21}$$

Sliding mode only occurs when all components of $\boldsymbol{s}$ in (20) are equal to zero instead of occuring in each component separately. Note that the control vector always has length τ_0, which led to the name *unit control* for this approach [1,4]. The stability analysis in the following theorem is also vector-based.

Theorem 1 [7]. The system (22) with bounds (4), (8), (9), and (10) under control (24) will reach the sliding manifold (23) in finite time:

System:

$$\ddot{\boldsymbol{q}} = \boldsymbol{M}^{-1}(\mathrm{t} - \boldsymbol{N}(\boldsymbol{q},\dot{\boldsymbol{q}}))\,; \tag{22}$$

Manifold:

$$\boldsymbol{s} = \boldsymbol{C}\boldsymbol{q}_e + \dot{\boldsymbol{q}}_e = \boldsymbol{C}(\boldsymbol{q}_d - \boldsymbol{q}) + (\dot{\boldsymbol{q}}_d - \dot{\boldsymbol{q}}) = 0\,; \tag{23}$$

Control:

$$\mathrm{t} = \tau_0 \frac{\boldsymbol{s}}{\|\boldsymbol{s}\|_2}\,. \tag{24}$$

Proof. Consider the Lyapunov function candidate:

$$V = \frac{1}{2}\boldsymbol{s}^T\boldsymbol{s}\,, \tag{25}$$

with its derivative along the system trajectories (22) under control (24):

$$\dot{V} =$$

$$= \boldsymbol{s}^T(\boldsymbol{C}\dot{\boldsymbol{q}}_e + \ddot{\boldsymbol{q}}_d - \boldsymbol{M}^{-1}(\boldsymbol{q}))\left(\tau_0\frac{\boldsymbol{s}}{\|\boldsymbol{s}\|_2} - \boldsymbol{N}(\boldsymbol{q},\dot{\boldsymbol{q}})\right)$$

$$\le -\frac{\tau_0}{M^+}\|\boldsymbol{s}\| + \|\boldsymbol{s}\|\left(\|\boldsymbol{C}\|\|\dot{\boldsymbol{q}}_e\| + \frac{N^+}{M^-} + \|\ddot{\boldsymbol{q}}_d\|\right). \tag{26}$$

Using the boundedness assumptions on (18) and using (4), (8), (9) and (10), we can find a sufficiently large τ_0 to guarantee:

$$\dot{V} \le -\xi\|\boldsymbol{s}\|_2\,, \tag{27}$$

and henceforth finite converge to the manifold $\boldsymbol{s} = \boldsymbol{0}_{n\times 1}$ in (23).

3.2.1 Vector control of two-link manipulator

Adaptation of the control design in Theorem 1 to the planar two-link manipulator example of (13) yields a sliding manifold:

$$\boldsymbol{s} = \begin{bmatrix} c_1 & 0 \\ 0 & c_2 \end{bmatrix}\begin{bmatrix} q_{e_1} \\ q_{e_2} \end{bmatrix} + \begin{bmatrix} \dot{q}_{e_1} \\ \dot{q}_{e_2} \end{bmatrix}, \tag{28}$$

which is used for choice of gain matrix:

$$\boldsymbol{C} = \begin{bmatrix} c_1 & 0 \\ 0 & c_2 \end{bmatrix}. \tag{29}$$

The difference in control design becomes apparent when defining the vector controller according to (24), as:

$$\mathrm{t} = \tau_0 \frac{\boldsymbol{s}}{\|\boldsymbol{s}\|_2} = \tag{30}$$

$$= \frac{\tau_0}{[(c_1 q_{e_1} + \dot{q}_{e_1})^2 + (c_2 q_{e_2} + \dot{q}_{e_2})^2]^{1/2}}(Cq + \dot{q})\,.$$

Stability can be established using Lyapunov function candidate:

$$V = \frac{1}{2}\boldsymbol{s}^T\boldsymbol{s} = \frac{1}{2}(s_1^2 + s_2^2)\,. \tag{31}$$

Differentiation along the system trajectories (13) with manifold (28) and under control (30) yields:

$$\dot{V} = s_1\dot{s}_1 + s_2\dot{s}_2 = -\frac{\tau_0}{M^+}\|\boldsymbol{s}\| + \tag{32}$$

$$+ \|\boldsymbol{s}\|\left(\sqrt{c_1^2\dot{q}_{e_1}^2 + c_2^2\dot{q}_{e_2}^2} + \frac{N^+}{M^-} + \sqrt{\ddot{q}_1^2 + \ddot{q}_2^2}\right).$$

Substituting the matrix bounds of the example in Section 2.1 leads to an upper bound on the required control resources as:

$$\tau_0 \ge$$

$$\ge M^+\left(\sqrt{c_1^2\dot{q}_{e_1}^2 + c_2^2\dot{q}_{e_2}^2} + \frac{N^+}{M^-} + \sqrt{\ddot{q}_1^2 + \ddot{q}_2^2}\right) +$$

$$+ \xi,\ (\xi > 0)\,. \tag{33}$$

The desired link acceleration $\|\boldsymbol{q}_d\| = \sqrt{\ddot{q}_{d_1}^2 + \ddot{q}_{d_2}^2}$ may be substituted for the actual link acceleration $\|\boldsymbol{q}\| = \sqrt{\ddot{q}_1^2 + \ddot{q}_2^2}$ under the assumption of exact tracking. Note that vector control design requires *both* joints to provide resources according to (33).

Simulation results are shown in Figure 4.

WORKSPACE TRAJECTORY

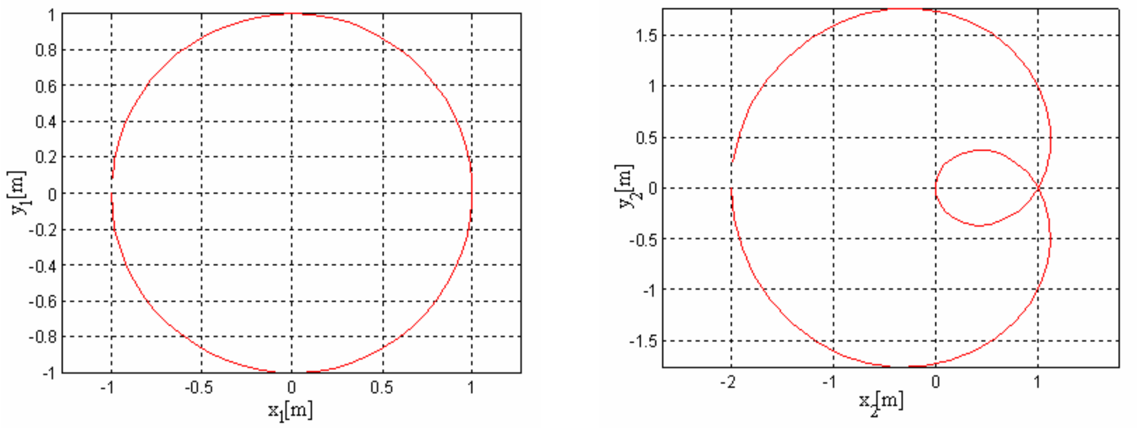

Fig. 4. Robot trajectories in world coordinates for vector control design.

4. CONCLUSIONS

In this paper, we have presented the use of sliding mode control strategy for the trajectory tracking control of the one, of the most employed manipulators in industrial enviroments, especially for assembly tasks. Results presented in the paper are important from a practical point of view since they provide a detailed framework about the design of the control structure for the trajectory tracking task.

REFERENCES

[1] Dorling, C., Zinober, A.S.I., *Two Approaches to Hyperplane Design in Multivariable Variable Structure Control Systems*, Int. J. Control, Vol. 44, No. 3, pp. 65-82, 1986.

[2] Harashima, F., Xu, J-X., Hashimoto, H., *Tracking Control of Robot Manipulators Using Sliding Mode*, IEEE Trans. Power Electronics, Vol. PE-2, No.2, pp.169-176, 1987.

[3] Nakamura, Y., Chung, W., Sordalen, O.J., *Design and Control of the Nonholonomic Manipulator*, IEEE Trans. Robotics and Automation, Vol. 17, No.1, pp. 48-59, 2001.

[4] *Discontinuous Feedback Control*, IMA J. Mathematics, Control and Information, Vol. 1, pp. 223-242, 1984.Slotine, J-J.E., Sastry, S.S., *Tracking Control of Non-linear Systems Using Sliding Surfaces, with Application to Robot Manipulators*, Int. J. Control, Vol. 38, No.2, pp. 465-492, 1983.

[5] Utkin, I.V., *Sliding Modes in Control Optimization*, Springer-Verlag, Berlin, Germany, 1992.

[6] Utkin, I.V., Güldner, J., Shi, J., *Sliding Mode Control in Electromechanical Systems*, Taylor & Francis Ltd., London, United Kingdom, 1999.

[7] Visioli, A., Legnani, G., *On the Trajectory Tracking Control of Industrial SCARA Robot Manipulators*, IEEE Trans. Ind. Electronics, Vol. 49, No.1, pp.224-232, 2002.

[8] Young, K-K.D. (ed.), *Variable Structure Control for Robotics and Aerospace Applications*, Elsevier Science Publishers B.V., Amsterdam, The Netherlands, 1993.

[9] Ryan, E.P., Corless, M., *Ultimate Boundedness and Asymptotic Stability of a Class of Uncertain Systems via Continuous and*